A MODELLING STUDY OF SEAWATER INTRUSION IN THE LIAO DONG BAY COASTAL PLAIN, CHINA

Fei Ding[1,2], Takao Yamashita[2], Han Soo Lee[2] and Jun Pan[3]

Key words: seawater intrusion, groundwater, SEAWAT code, Liao Dong Bay.

ABSTRACT

To investigate the extent of seawater intrusion in the Liao Dong Bay coastal plain, China, a numerical model for variable-density groundwater flow and miscible salt transport was developed. The SEAWAT code was used to solve the density-dependent groundwater flow and solute transport governing equations. The simulation was conducted for 55 months from October, 2004 to April, 2009. The numerical model was calibrated by the hydraulic heads measured in April, 2009. Using the calibrated model and the same hydrogeological conditions in 2004, the extent of seawater intrusion prediction was conducted for the next 40 years. The results show that the extent of seawater intrusion area will increase in all geologic layers with nearly 6.2 km in the upper Quaternary aquifer and 4.3 km in lower Quaternary aquifer for 40 years. In the Minhuazhen group aquifer, the maximum speed of seawater intrusion is 62.2 m/yr. Therefore, some protection of the freshwater aquifer from seawater intrusion in the Liao Dong Bay coastal plain is imperative.

I. INTRODUCTION

Seawater intrusion is the movement of ocean water into fresh groundwater due to the natural processes or human activities. With the fast-growing economy in the coastal regions, the demands for water resource and the exploitation of groundwater have been increased. There have disturbed the established balance between fresh water and seawater, causing extensive seawater intrusion into groundwater.

A number of mathematical and numerical models have been

developed and used to predict the location and movement of the seawater intrusion. Depending on the method of treating the interface for simulation, these models can be grouped into two broad categories: sharp interface and variable density models where a wide interface zone separates the two fluids [1, 12, and 21]. The sharp interface assumption can be applied only under certain the conditions when the width of the transition zone is relatively small compared with the thickness of the aquifer.

The phenomenon of freshwater underlain by saltwater is quite a complex one. Fresh water and salt water are miscible fluids, and a transition zone always exists between them in coastal aquifers [9]. In reality the two fluids are separated by a transition zone with a continuous upward gradient of salt concentration from saltwater below to uncontaminated above [12]. The transition zone will move landwards when seawater intrusion occurs. The variable density model that accounts for the effects of hydrodynamic dispersion may be more practical as it provides more details concerning the transition zone [1]. Therefore, most of the simulation codes have been developed based on the variable density theory. Several computer codes that can be used to simulate density-dependent groundwater flow have been developed [33]. In the last decade, there were several density-dependent simulation codes developed based on the commonly-used groundwater model [27] MODFLOW which was developed by the U.S. Geological Survey [18, and 29]. The major and commonly-used MODFLOW-based computer codes are SEAWAT [16, 17, and 22], MOCDENS3D [31], MODHMS [14] and the Sea Water Intrusion Package for MODFLOW [8]. All these codes can been applied to case studies and have been documented and tested with variable-density benchmark problems. A summary of these four codes was reviewed by Langevin et al. [23].

A number of case studies on seawater intrusion based on variable density theory in coastal area have been done. Andersen et al. [2] used a finite element model SWICHA [19] to simulate salt water intrusion in Hallandale, located on the east coast of Florida. A numerical simulation on saltwater intrusion in the unconfined coastal aquifer of Ravenna (Italy) was made by Giambastiani [15] with the MOCDENS3D code. El-Bihery [13] numerically simulated seawater intrusion of Quaternary aquifer in Ras Sudr, Egypt by using MODFLOW code and SEAWAT. Lin et al. [27] used SEAWAT code to solve a variable-density groundwater flow and miscible salt transport numerical model to investigate the extent of seawater intrusion

in the Gulf coast aquifers of Alabama, USA. Kopsiaftis et al. [21] constructed a quasi-three-dimensional variable density transport model for the unconfined aquifer located in the central part of Thira Island (Santorini) using the iterative solving method by software package of FEFLOW. Bhosale used SUTRA [34] model to simulation of seawater intrusion in Ernakulam coast [10].

The FEFLOW, SUTRA, and SEAWAT have been applied on a variety of real-world and analytical problems. SUTRA (Saturated-Unsaturated Transport) employs a two-dimensional finite-element approximation of the governing equations in space and an implicit finite-difference approximation in time. This model is suitable for a simulation of the vertical section of aquifer that is subject to seawater intrusion. On the other hand, FEFLOW is a finite-element package for simulating 3D and 2D fluid density-coupled flow, contaminant mass (salinity) and heat transport occurring in the subsurface. It evaluates the impact of seawater intrusion caused by groundwater pumping and/or mining activities along coastal regions [10]. The SEAWAT program is a coupled version of MODFLOW and MT3DMS designed to simulate three dimensional finite-difference, variable-density and saturated ground-water flow. Flexible equations were added to the program to allow fluid density to be calculated as a function of one or more MT3DMS species [25]. While FEFLOW and SEAWAT allow transport for more than one solute, as is required for simulation of contaminant migration in the variable density flows of coastal aquifers, SEAWAT is the more readily available of these codes, being available free of charge from the U.S. Geological Survey (U.S. Geological Survey, 2004) [14, 17].

In 2007, the State Oceanic Administration of People's Republic of China started monitoring seawater intrusion in China. The activity helped established the fact that seawater intrusion is in serious level condition particularly in Liao Dong Bay area (Fig. 1) where coverage of seawater intrusion area is more than 4,000 m^2 with serious intrusion area of nearly 1,500 m^2. The most remote region of seawater intrusion is 68 km far from the shore in Panjin City. (See the web site, http://www.soa.gov.cn /hyjww/zghybnew/tkb/webinfo/2008/01/1200912281939611.h tm). It is significant task to make clear the seawater intrusion and to predict its extending area in Liao Dong Bay coastal plain by numerical study. Li [26] employed the software of Visual MODFLOW for the first time to study numerical seawater intrusion in the upper Neozoic layer of the Liaohe Oil Field which is located in the south of the lower Liaohe Plain. Xue [36] conducted the simulation of groundwater level in the upper Neozoic using Visual MODFLOW in Pan Jing area. For seawater intrusion problem, spatial variations in fluid density can markedly affect ground water flow patterns [24]. In previous model studies [26, 36] of Liao Dong Bay coastal plain area, they used Visual MODFLOW software to calculate the quasi-three-dimensional flows which have not considered groundwater density variable and Quaternary layer salt water effect.

This study deals with numerical model on seawater intrusion in Liao Dong Bay coastal plain based on SEAWAT which is a quasi-three-dimensional variable-density numerical code. This simulation considers both the groundwater layers of Quaternary and upper Neozoic. Compared with previous studies, this model improved in two parts. It considered groundwater density variable and seawater intrusion in Quaternary and Neozoic layers. The total simulation period is 55 months from October, 2004 to April, 2009. After the model calibration by using the observation data in April 2009, the calibrated model was used to predict the extent of seawater intrusion for 40 years to come assuming the same conditions in 2004.
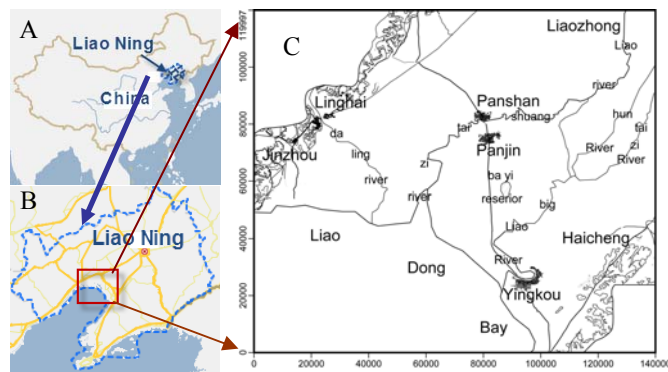

Fig. 1. A: Location of Liao Dong Bay coastal plain, China. B: blue line indicates Liao Ning and red line the study area. C : the simulation domain. (unit in meter).

This paper consists of four sections, as follows. Section 2 describes the background of Liao Dong Bay coastal plain. In Section 3, numerical modelling of seawater intrusion was designed. In Section 4, the results of model calibration and prediction of seawater intrusion in the Liao Dong Bay coastal plain are described. Finally, Section 5 provides summary and conclusions of this study.

II. BACKGROUND OF LIAO DONG BAY COASTAL PLAIN

1. Site Description

The Liao Dong Bay coastal plain is located in the south of Liao Ning province, China. The major study area is Pan jing city and a part of Yingkou city, Jinzhou city and Haicheng city as shown in Fig. 1. This area is rich in surface water, but the rainfall runoff has been decreasing year by year and water quality has been degraded. About 50% of the city water and 100% industrial water depend on the groundwater in this area [11].

The average annual temperature is 8.4 °C. The average maximum temperature is 23.8 °C in the summer and -9.7 °C in winter respectively. The average annual rainfall is 647.4 mm/year. Most of the rainfall occurs in the summer from June to September, that is about 63% of the annual precipitation. The average annual evaporation is 1,568.6 mm/year.

The study area is located in the central and southern Liao Dong Bay coastal Plain. The terrain is flat and the north area is higher than the south area. The northern elevation is from 5 to 7

m and most of the southern part is below 5 m. The terrain is sloping from northeast to southwest and the average hydraulic gradient is 0.02 ‰.

2. Stratigraphy

The subsurface stratigraphy of the study area consists of sedimentary rocks ranging from the Cenozoic to Holocene in age. There are two stratigraphies in the Quaternary stratigraphy and Neozoic stratigraphy in the study area. The generally east–west cross-section was constructed based on the geologic information as well as geologic data from several drilled wells as shown in Fig. 2, where drilled wells are shown as LP14 ect [26, 35 and 36].

1) The Quaternary Stratigraphy

In the study area, the Quaternary stratigraphy development was essentially completed with thickness ranges from 65 to 400 m [11, 26, 35, and 36]. The Quaternary stratigraphy from top to bottom developed in the ages of Holocene, upper Pleistocene, middle Pleistocene and lower Pleistocene, and the corresponding genetic types of deposits are alluvium-marine, alluvium, alluvium-diluvium, and diluvium. Quaternary stratigraphy from the new to the old is described as follows :

Holocene Stratigraphy (Q_{4p}): It is Alluvium-marine. The underlying layer is Pleistocene alluvium with thickness between 10 and 15 m. It consists of a yellowish brown to grayish brown Middle-fine to fine sand, clay and silt. At piedmont alluvial-pluvial fan, the major portion consists of sand and gravel with thickness between 10 to 170 mm and quartz based mineral composition.

Upper Pleistocene Stratigraphy (Q_{3y}): The Upper Pleistocene stratigraphy underlies the Holocene sediments and overlies the Middle Pleistocene alluvial sediments. It is between 50 and 60 m thick. Lithology is mainly fine sand or sub-clay in the coarse sand lens sub-folder and the color is gray, gray and yellow, and taupe. The plasticity of sub-clay is strong loam, and iron disseminated widely. Fine sand or coarse sand is good sorted rounded, mainly consist of quartz, feldspar and so on. There is stable sub-clay layer at the top of Upper Pleistocene layer.

Middle Pleistocene Stratigraphy (Q_{2z}): The Middle Pleistocene stratigraphy underlies the Upper Pleistocene alluvium sediments on the system and has a thickness between 40 and 50 m thick. Lithology is mainly coarse sand, fine sand and clay sub sandwich. The color is gray, grayish yellow or gray-green. Fine sand, coarse sand sorting rounded is normal, the main mineral composition of quartz and feldspar. Sand distribution is more continuous while sub-clay layers are discontinuous. There is no recognizable divides between Upper Pleistocene layer and Middle Pleistocene layer.

Lower Pleistocene Stratigraphy (Q_{1x}): The lower Pleistocene stratigraphy underlies the Middle Pleistocene alluvium sediments and has a thickness of more than 20 m. Lithology is gravel mixed sub-clay and there are thin layers of sub-clay in some area. There is stable sub-clay layer at the top and bottom of lower Pleistocene layer. The color is gray, gray and yellow, dark grey.
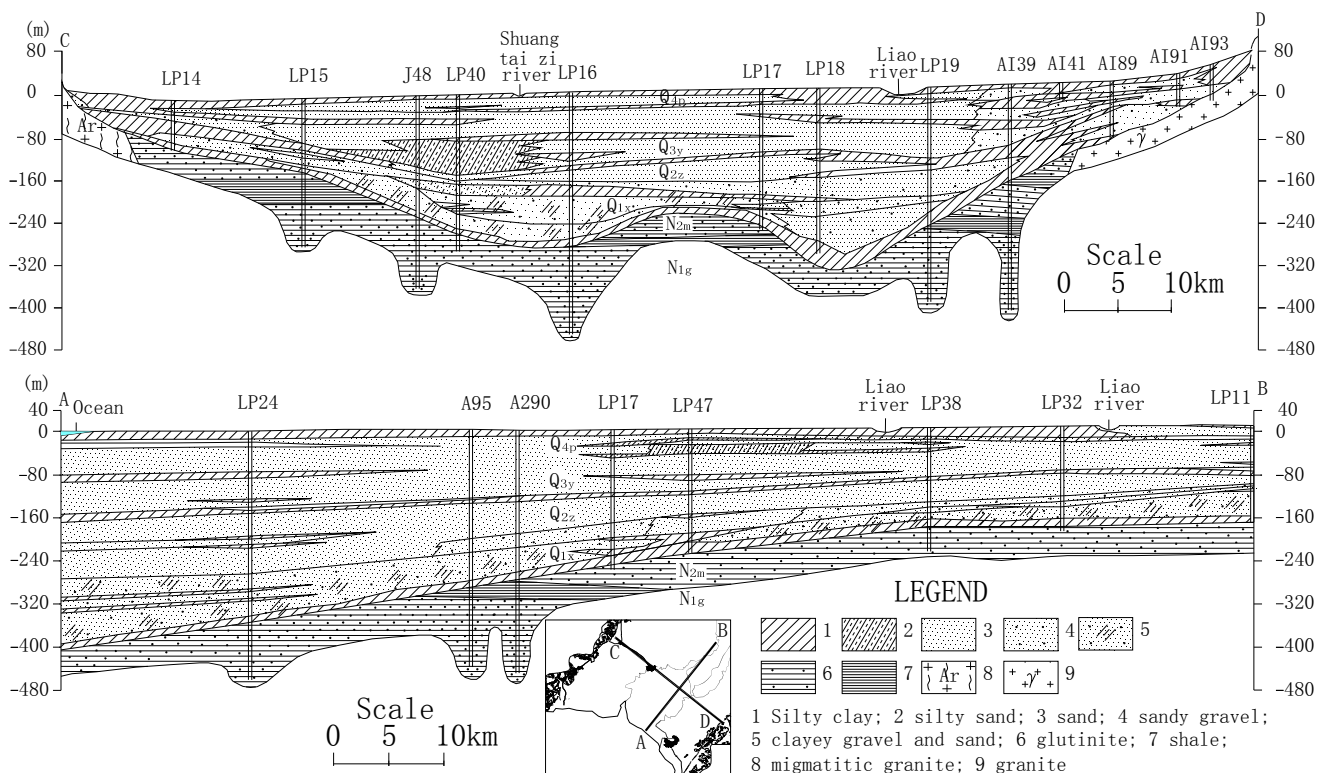

1 Silty clay; 2 silty sand; 3 sand; 4 sandy gravel; 5 clayey gravel and sand; 6 glutinite; 7 shale; 8 migmatitic granite; 9 granite

Fig. 2. Geologic cross-sections of the study area

Table 1. Hydrogeologic units.

Hydrogeologic unit		Unit character	
Aquifer zone	Geologic interval units	Lithologic	Hydrologic
A1 (Quaternary)	Holocene (alluvium-marine)	Sand, yellowish brown to grayish brown, middle-fine to fine sand, clay and silt.	Sand and gravel in unit comprise major aquifers. The upper aquifers is unconfined aquifer and the lower aquifers are generally semiconfined. At east, west and northern of the study area is major freshwater, Potential soure of 5,000 to 7,000 m³/day of water per well. Salt water general distribute in the mid-south coastal plain. Potential soure of 100 to 1,000 m³/day of water per well.
	Upper Pleistocene (alluvium)	Sand, gray, gray and yellow, taupe, fine sand or sub-clay in the coarse sand lens sub-folder. There is stable sub-clay layer at the top it.	
A2 (Quaternary)	Middle Pleistocene (Alluvium-Diluvium)	Sand, gray, grayish yellow or gray-green, coarse sand, fine sand and clay sub sandwich. Sub-clay layers are discontinuous.	
	Lower Pleistocene (Diluvium.)	Sand, gray, gray and yellow, dark gray, gravel mixed sub-clay. There is stable sub-clay layer at the top and bottom of lower Pleistocene layer.	
A3 (Upper Neozonic)	Minghuazhen group	Mudstone and argillaceous siltstone. It is impermeable layer.	The thickness is more than 3 m.
A4 (Upper Neozonic)	Minghuazhen group (lacustrine sediment)	The top belt is the white sandrock from semi-coarse to semi-fine particle, conglomerate with sand and sandrock with gravel. The bottom belt is gray green, yellow brown development bedding and plant detritus is composed of mudrock, conglomerate with sand.	Sandstone and pebbly sandstone in unit comprise major aquifers. The aquifers are generally confined. Potential soure of 33.4 to 4,689 m³/day of water per well.
A5 (Upper Neozonic)	Guantao group (coarse clastic fluvial facies deposits)	Gray-white, light gray green conglomerate with boulders, small conglomerate, pebbly sandstone, sandstone mudstone. There are the gray green mudstone, muddy silt layer or lens.	Sandstone and conglomerate in unit comprise major aquifers. The aquifers are generally confined. Potential soure of 273 to 4,992 m³/day of water per well.

In summary, the Quaternary sedimentary rhythm in the study area is clear and cyclic. The Holocene, upper Pleistocene and middle Pleistocene deposits have two or more cycles. Because of the tectonic movement, the middle Pleistocene deposit in this area extended toward further northwest than the lower Pleistocene deposit and the Holocene deposit extended further toward northwest than the middle Pleistocene deposit. This is the overlap of the stacking features.

The Neogene stratigraphy consists of upper Neozoic stratigraphy and lower Neozoic stratigraphy. The upper Neozoic sedimentary is thicker and is divided into Minghuazhen group (N_{2m}) and Guantao group (N_{1g}) formations. There are volcanic and volcaniclastic rocks with the foot and fluvial-lacustrine clastic deposits. The fault is well-developed and sedimentation distribution is not uniform. Under the function of different sedimentation, there are seven high-angle normal faults and the separation is 10 to 145 m. These faults broke thrust the Minghua and Guantao formation [11, 26, 35, and 36].

Minghuazhen Stratigraphy (N_{2m}): The Minghuazhen group is a lacustrine sediment divided into two belts. The top belt of the Minghuazhen group formation forms a white sandrock from semi-coarse to semi-fine particle, conglomerate with sand and sandrock with gravel. The particles were sorted well, gravel diameter is 0.5 to 20 mm, which became slender from north to south. The bottom belt of the Minghuazhen group is gray green, yellow brown development bedding and plant detritus is composed of mudrock, conglomerate with sand. The mudrock is attributed in the upper apex and partial deletion with thickness from 4 to 8 m. The embedded depth of the formation is between 100 to 400 m with shallow portion from bilateral east-west to middle and deeper part from northeast to southwest [11].

Guantao Stratigraphy (N_{1g}): Guantao stratigraphy lies under the Minghuazhen group Formation with a set of coarse clastic fluvial facies deposits, lithology single, gray-white, light gray green conglomerate with boulders, small conglomerate, pebbly sandstone, sandstone mudstone, there are the gray green mudstone, muddy silt layer or lens. Gravel diameter is generally 3 - 10mm. The particles are sorted poor. The embedded depth of the formation is between 350 to 1,200 m with shallow portion from bilateral east-west to middle and deeper portion from northeast to southwest. The thickness of the formation is generally 50 - 370 m with thicker and deeper layer from bilateral east-west to middle and from northeast to southwest. In the eastern and western of study area, the Guantao stratigraphy is missing.

The lower Neozoic is located below the upper Neozoic. The upper part forms Dongying group formation (E_d) lithology which mainly consists of white, light gray sandstone and glutenite, variegated mudstone. Its thickness ranges 200 to 1,600m. The bottom layer is Shahejie group formation (E_s) which has a complex lithology.

3. Hydrogeology

Due to the high degree of variability and lateral discontinuity within the geologic units, aquifer zones are determined upon their hydrogeologic characteristics. Hydrogeologic units, utilized as groundwater sources in the study area, are described in Table 1.

Major groundwater source occurrences are in the Quaternary layer with unconsolidated rock porosity and in the upper Neozoic clastic rocks layer with the fracture and the pores, in study area. The regional groundwater flow is mainly from north to the Liao Dong Bay Sea, from west and east mountain area to the middle plan area.

1) Quaternary Pore Water

The Quaternary loosened deposits generally cover the whole study area. Its maximum thickness reaches to 370 m. The major recharge of groundwater is vertical infiltration and the major discharge is evaporation and artificial pumping.

At the east and west sloping piedmont in the study area, groundwater mainly exists in alluvium and alluvium-diluvium sand, gravel, sandy gravel and sandy gravel mixed soil pores. The thickness of its aquifer ranges from 70 to 160 m with hydraulic conductivity between 20 to 115 m/day and groundwater depth from 3 to l0 m. The potential water source per well is 7,000 m³/day in this rich water resource region. In the alluvial plains on the northern study area, the main occurrence of groundwater occurs in the fine sand of marine red, medium-fine sand, gravel, sand and gravel mixed soil pores. The aquifer has a thickness which ranges from 150 to 280 m, a hydraulic conductivity between l2 to 20 m/day, a groundwater depth from l to 4 m, and a potential water source per well of 5,000 m³/day.

Salt water is generally distributed in the mid-south coastal plain where the groundwater mainly exists in alluvium-marine silt, fine sand, fine sand, sand and gravel pores. In this water resource generic region, the thickness of the aquifer ranges from 70 to 360 m, the hydraulic conductivity is 8 to 14 m/day, the groundwater depth is 0.5 to 3 m, and the potential water source per well is 100 to 1,000 m³/day.

2) The Upper Neozoic Pore-crack Groundwater

The upper Neozoic water is divided into Minhuazhen group and Guantao group. Freshwater exists in medium-grained sandrock and conglomerate accumulated in rivers and lakes.

Minhuazhen Group Groundwater: The major recharge of groundwater in Minhuazhen group comes from the rainfall runoff of adjacent aquifer, the vertical infiltration of groundwater in the Quaternary layer, and the lateral recharge in an old foundation base. The natural flow field of groundwater reflected the runoff flows slowly from east and west bilaterally and north to southwest. In exploiting condition, the groundwater flow direction is changed and the all surrounding groundwater is collected into the center. In natural condition, the groundwater discharges itself to southwest and the artificial withdrawal is only the discharge way.

Minhuazhen group groundwater consists of freshwater region and salt water region. Saline water is divided into three zones, namely, whole saline water zone, the upper saline, and the lower fresh water zone. The whole saline water zone is distributed in the middle of the saline water zone. Its chlorine concentration is more than 1,000 mg/l. The upper saline and the lower fresh water zone is distributed around the whole saline water zone, where is the transition belt of the saline and fresh water as shown in the Fig. 10(B). Its chlorine concentration is more than 250 mg/l. Minghuazhen group salt water occurs in the river and lake facies, paludal facies of siltstone, fine sandstone, fine sandstone, coarse sandstone and pebbly sandstone layer, and the water depth ranges from 230 to 450 m,

Minhuazhen group freshwater mainly occurs in fluvial facies, river and lake facies stratum of coarse sandstone, sandstone, pebbly sandstone and conglomerate. Its roof depth ranges from 100 to 990 m, and the aquifer thickness is between l0 to 900 m.

Guantao Group Groundwater: A major Guantao group groundwater occurrence is in the fluvial facies deposits, pebbly sandstone, conglomerate, fine conglomerate, and conglomerate boulder with a small amount of pores and cracks. The rock cementation is poor and its aquifer thickness ranges from 14 to 350 m. Groundwater level is generally -5 to -40 m. The confined aquifer has a hydraulic conductivity of 0.8 to 9.2 m/day and the potential water yield per well is 273 to 4,992 m^3/day.

4. Likely Causes of Seawater Intrusion

The first cause is the natural seawater intrusion in the layers of primary sedimentary of marine bed. There exists the several periods of seawater intrusion into Liao Dong Bay coastal plain due to earth crust uplift and down-welling since the Neozoic. After the occurrence of the seawater intrusion, in each period a large amount of marine sediment deposited. This is the major cause of salt water intrusion into Liao Dong Bay coastal plain in which some original salt water is retained.

The second cause is anthropogenic one. The increasing population subsequently caused the excessive exploitation of groundwater which damaged the water balance of salt water and freshwater, resulting in the increase of seawater intrusion. In Ying Kou City and Jing Zhou City, due to an excessive exploitation of groundwater, the groundwater level has continued to decline, particularly in the region of Ying Kou City where the freshwater table has reached below the sea level in the funnel region.

In Liao Dong Bay coastal plain, there were three steps of large-scale transgression of layers since the Quaternary period. The first is the Pan Shan transgression layer in mid-Holocene with thickness from 8 to 34 m. The second is the Pioneer transgression layer in lower Pleistocene with thickness from 44.6 to 79.1 m. The third is the water resource transgression layer in middle Pleistocene with thickness from 89.2 to 161.8 m. All of the ground water contains salt water in the Quaternary layer in the south of Pan Shan area.

For the salt water in Neozoic period, according to the analysis of the environment of salt water occurrence media, underground salt water distribution, water chemistry and environmental isotope characteristics, it was found out that the original underground salt water of Minghuazhen group is from precipitation, and its origin has no connection with the sea water. The salt water of Minghuazhen group was sealed off from the residual of lake water after its evaporation in the continental deposition environment [26].

III. NUMERICAL MODELLING

1. Simulation Code

SEAWAT code is a useful tool for simulating various types of variable-density fluid flow through complex geometries and geological settings, including seawater intrusion in coastal aquifers, submarine groundwater discharge, brine transport, and groundwater flow near salt domes [27].

In this study, SEAWAT code capable of simulating quasi-three-dimensional variable-density groundwater flow in porous media was used to simulate the seawater intrusion into the coastal aquifers in Liao Dong Bay coastal plain. The fundamental concept of this code is to combine the two commonly-used groundwater flow and solute transport modeling programs of MODFLOW [18] and MT3DMS [37]. These were combined into a single program that solves the basic equations for density-dependent groundwater flow and solute-transport.

The governing equation for density-dependent groundwater flow in terms of freshwater head, which is solved by MODFLOW routines in SEAWAT code [17, 27] is as follows:

$$\frac{\partial}{\partial \alpha}\left\{\rho K_{f\alpha}\left[\frac{\partial h_f}{\partial \alpha}+\frac{\rho-\rho_f}{\rho_f}\frac{\partial Z}{\partial \alpha}\right]\right\}+\frac{\partial}{\partial \beta}\left\{\rho K_{f\beta}\left[\frac{\partial h_f}{\partial \beta}+\frac{\rho-\rho_f}{\rho_f}\frac{\partial Z}{\partial \beta}\right]\right\}$$
$$+\frac{\partial}{\partial \gamma}\left\{\rho K_{f\gamma}\left[\frac{\partial h_f}{\partial \gamma}+\frac{\rho-\rho_f}{\rho_f}\frac{\partial Z}{\partial \gamma}\right]\right\}=\rho S_f\frac{\partial h_f}{\partial t}+\theta\frac{\partial \rho}{\partial C}\frac{\partial C}{\partial t}-\overline{\rho}q_s \quad (1)$$

where α, β, γ are orthogonal coordinate axes, aligned with the principal directions of permeability; $K_{f\alpha}$, $K_{f\beta}$, $K_{f\gamma}$, are equivalent freshwater hydraulic conductivities in the three coordinate directions, respectively [LT^{-1}]; ρ is the fluid density [ML^{-3}]; ρ_f is the density of freshwater [ML^{-3}]; h_f is the equivalent freshwater head [L]; Z is the elevation above datum of the center of a model cell [L]; S_f is the equivalent freshwater specific storage [L^{-1}]; θ is effective porosity [dimensionless]; C is the solute concentration [ML^{-3}]; $\overline{\rho}$ is the density of water entering from a source or leaving through a sink [ML^{-3}]; q_s is the volumetric flow rate of sources or sinks per unit volume of aquifer [T^{-1}]; and t is time [T].

The solute-transport governing equation of SEAWAT code utilizes MT3DMS routines [37] are as follows:

$$\frac{\partial C}{\partial t}=\nabla \cdot (D \cdot \nabla C)-\nabla \cdot (\upsilon C)-\frac{q_s}{\theta}C_s+\sum_{k=1}^{N}R_k \quad (2)$$

where D is the hydrodynamic dispersion coefficient [L^{2}T^{-1}]; $\overline{\upsilon}$ is the fluid velocity [LT^{-1}]; C_s is the solute concentration of water entering from sources or leaving through sinks [ML^{-3}]; and $R_k(k=1,...,N)$ is the rate of solute production or decay in reaction k of N different reactions [ML^{-3}T^{-1}].

For a coupled variable-density flow and solute-transport simulation, fluid density is assumed to be a function only of solute concentration; the effects of pressure and temperature on fluid density are ignored [22]. A linear equation of state is used by SEAWAT code to convert solute concentration to fluid density [17, 25]:

$$\rho = \rho_{\text{f}} + \frac{\partial \rho}{\partial C} C \qquad (3)$$

where $\partial \rho / \partial C$ is the slope of the equation. The value for $\partial \rho / \partial C$ is a dimensionless constant having an approximate value of 0.7143 for salinity concentrations ranging from zero to 35 kg/m^3 of seawater. For more details on SEAWAT, refer to its user's manual [17].

2. Model Discretization

In the plan view, the model grid consists of the grid system of 60 columns and 60 rows with uniform spacing of 2.0 km (NS-direction) and 2.33 km (WE-direction), respectively (Fig. 3).

In the vertical direction, the model grid consists of four layers representing the hydro-stratigraphy of Liao Dong Bay coastal plain (see Figs. 4 and 5). The right figure is the cross-section passing through Liao Dong Bay coast plain showing hydrogeologic units and vertical view of spatial discretization for the quasi-three-dimensional numerical model. For the left map, the red line shows the location of the cross-section, the green color area is the inactive area and the white area represents the active area.

Layer A1 corresponds to the Holocene (Q_{4p}) and Upper Pleistocene (Q_{3y}) Quaternary aquifers. Layer A2 corresponds to the Middle Pleistocene (Q_{2z}) and Lower Pleistocene (Q_{1x}) Quaternary aquifers. Layer A4 represents the Minhuazhen groupaquifer that is a confining layer. Layer A3 is an existing aquitard between layers A2 and A4 aquifer which is assumed
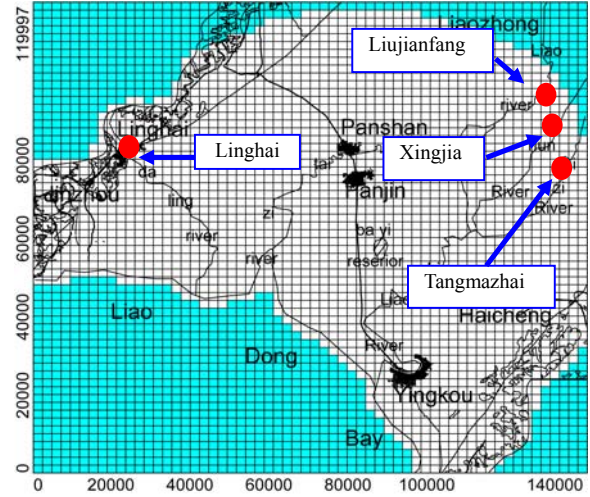

Fig. 3. Plan view of spatial discretization for the numerical model showing the inactive area (green) and the active area (white).

impermeable. In this model, the bottom boundary (A5) is set as Guantao group aquifer and lower Neozoic aquifer (See Table 1). Model layer thicknesses are determined by the occurrence of sand and clay layers documented in well driller's reports archived by the Liao Ning hydrogeology and engineering geology exploration institute [35].

A cross-section of the model from west to east is shown in Fig. 4, while Fig. 5 depicts a south to north cross-section of the Liao Dong Bay coastal plan. On both figures, units of distance and elevation are measured in meters, and the red line represents the location of the cross-section. While the green and the white cells indicate to the inactive and active computational
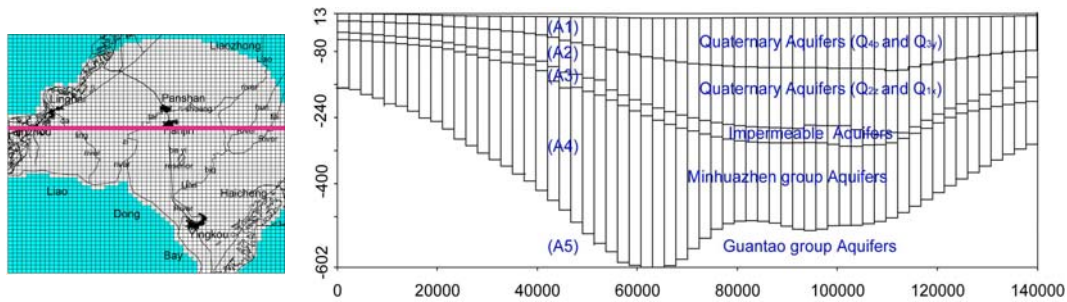

Fig. 4. The west to east cross-section showing the hydrogeologic units and vertical spatial discretization of the study area.
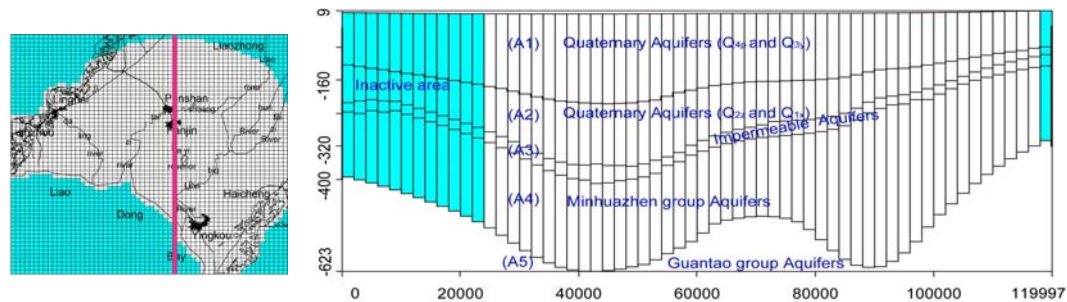

Fig. 5. The south to north cross-section showing the hydrogeologic units and vertical spatial discretization of the study area.

Table 2. Input parameters for the model and simulation strategies for this study.

Parameter	Layer A1	Layer A2	Layer A3	Layer A4
Hydraulic conductivity (K_x, m/day)	40～75	25～55	0.000432	4～10
Hydraulic conductivity (K_y, m/day)	40～75	25～55	0.000432	4～10
Hydraulic conductivity (K_z, m/day)	4～7.5	2.5～5.5	0.000013	0.4～1
Total porosity	0.23～0.3	0.23～0.3	0.000017	0.3
Effective porosity	0.15～0.25	0.15～0.25	0.000015	0.15
Specific storage	0.00018～0.00022	0.00018～0.00022	0.00001	0.0001～0.0002
Specific yield	0.18～0.22	0.18～0.22	0.001	0.15～0.23
Longitudinal dispersivity (m)	10～40	10～40	0.0027	10～35
Horizontal/Longitudinal dispersivity	0.1	0.1	0.1	0.1
Vertical/Longitudinal dispersivity	0.01	0.01	0.01	0.01
Molecular diffusion (m^2/s)	1.0×10^{-9}	1.0×10^{-9}	1.0×10^{-9}	1.0×10^{-9}
Freshwater density (kg/m^3)	1000	1000	1000	1000
Seawater density (kg/m^3)	1025	1025	1025	1025
Constant head (m)	2			
Recharge concentration (mg/L)	0			
Constant head concentration (mg/L)	7000～12000	6500	6500	
Initial Concentration	Based on observation data			
Recharge	Based on observation data			

cells, respectively.

A total of 55 stress periods, from October, 2004 to April, 2009, is used in the model simulation with the time step of 1 month.

3. Hydrogeological parameters

The zoning map of the hydraulic conductivity was created using the data determined by pumping tests conducted at the time of well completion and recorded in well driller's logs. All hydraulic conductivities are used with averaged values in each zone. Considering the size of zone, model's hydraulic conductivities were adjusted during model calibration. Representative properties of the study area (Table 2) were assigned to the model cells. Hydraulic conductivity of the aquitards was determined to be 4.32×10^{-4} m/day in Layer A3 and assumed to be constant inside the whole aquitard. The vertical hydraulic conductivities in all the layers were assumed to be 10% of the horizontal hydraulic conductivity.

Recharge was applied to the most active upper layer. Monthly precipitation data was obtained from the China Meteorological Data Sharing Service System. From annual evapotranspiration data, an averaged evapotranspiration rate was calculated as 4.298×10^{-4} m/day.

The effective porosity was set at 0.15 to 0.25 as an initial guess. The longitudinal dispersivity was set at 10 to 40 m in the flow system based on the injecting tests conducted at the time of well completion (from the well driller's logs). The ratio of horizontal transverse dispersivity to the longitudinal disper-

sivity was assumed to be 0.1. On the other hand, the ratio of the vertical transverse dispersivity to the longitudinal dispersivity was assumed to be 0.01. As needed, these values were adjusted during the model calibration.

4. Boundary and initial conditions

Since the model was set up to simulate the seawater intrusion into the coastal aquifers, both groundwater flow and solute transport processes were simultaneously involved with consideration of the boundary conditions. For the flow computation, the boundary conditions (Fig. 6) were set as constant head boundary with crimson line in Layer A1 (Fig. 6(a)) which was set by the no-flow boundaries (Fig. 6(a), pink line) at the northwestern and southeastern mountain edges. The blue color line is river boundary. The specified hydraulic head values either 2 m (the mean sea level) or interpolated values from the measured water heads along the boundaries. The flow boundaries of layers A2 and A4 were set as constant head boundary according to the observe data in October, 2004. The green color area is the inactive area and the white color area represents the active area.

Streams and rivers (Fig. 6(a), blue line) were specified with the river package of the SEAWAT code. Width, depth, and river stage of river water were determined from the observed data in Linghai, Liujianfang, Tangmazhai and Xingjia stations (Fig. 3) while the width, depth and river stage at the river mouth are determined from topographic maps. Based on the stations observed data and river mouth data, each part of river width, depth,
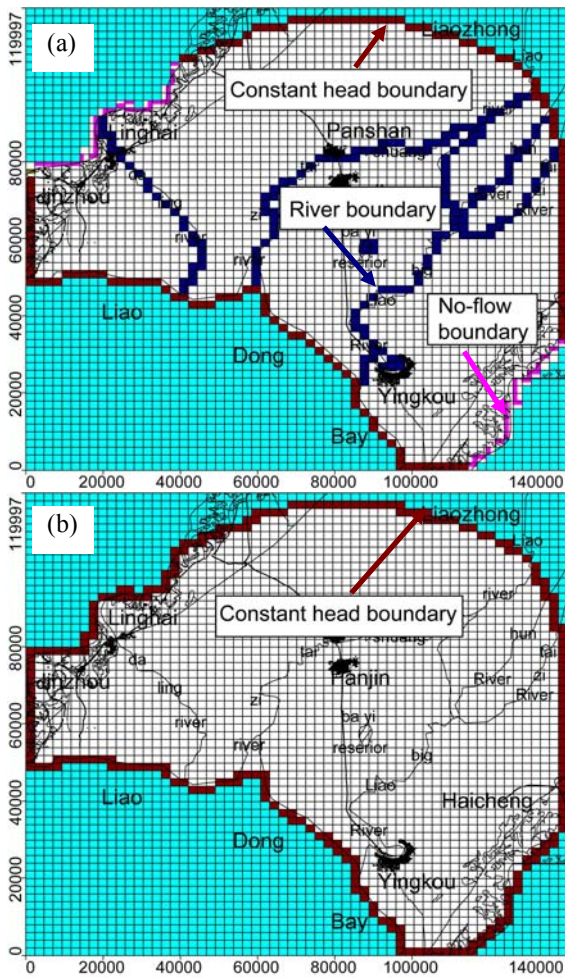
and river stage was then interpolated.

Fig. 6. Flow boundary conditions for each layer of the numerical model: (a) Layer A1, and (b) Layers A2 and A4.

The concentration level of Total Dissolved Solids (TDS), Sodium (Na) and Chloride concentration (Cl) are normally used as verifiable indicators for seawater intrusion. However, due to the lack of data on TDS and Na, chloride concentration is considered as the simulated component in this study for the solute transport computation. In addition, seawater intrusion can be observed if at any specific location in the aquifer the chloride concentration rises above 0.25 kg/m^3 as set forth by the Ministry of health. [30]. The chloride concentration in seawater is approximately 12 kg/m^3. In the Layers A1, A2 and Layer A4, the boundary conditions are set as the Constant concentration boundary (Fig. 7). As the A1 aquifer is in contact with the surface water, chloride concentration along the coast was specified at 12 kg/m^3 (Fig. 7(a), lightblue line), and 7 kg/m^3 (Fig. 7(a), green line) in the river mouth area where mixing of freshwater with seawater was considered. Chloride concentration along the coast was set as 6.5 kg/m^3 in the A2 aquifer. Salt concentration of river water was determined from the observed data in Linghai, Liujianfang, Tangmazhai and Xingjia stations (see Fig. 3). And each part river chloride concentration can be interpolated between the stations ob-

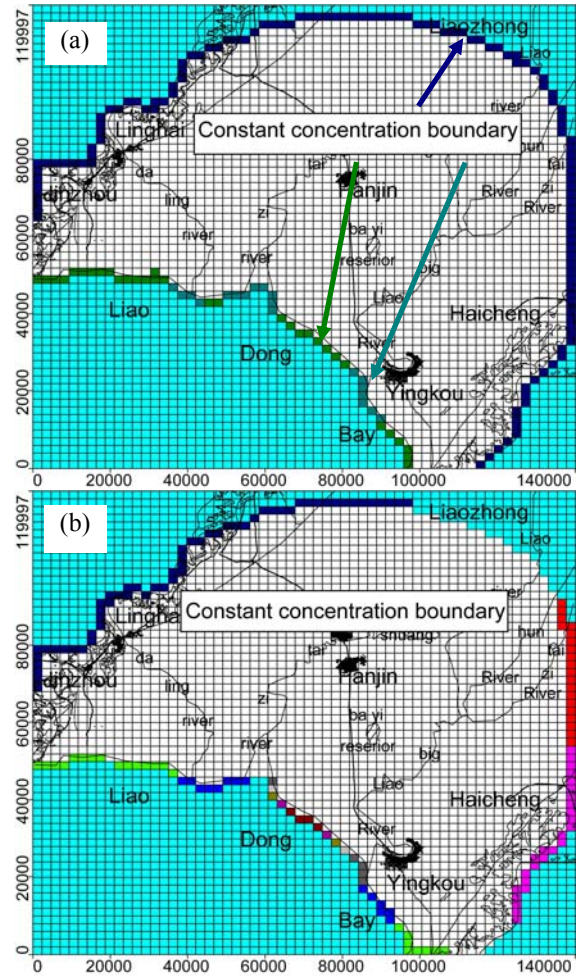served data and river mouth data. On the

Fig. 7. Transport boundary conditions for each layer of the numerical model: (a) Layer A1, and (b) Layers A2 and A4.
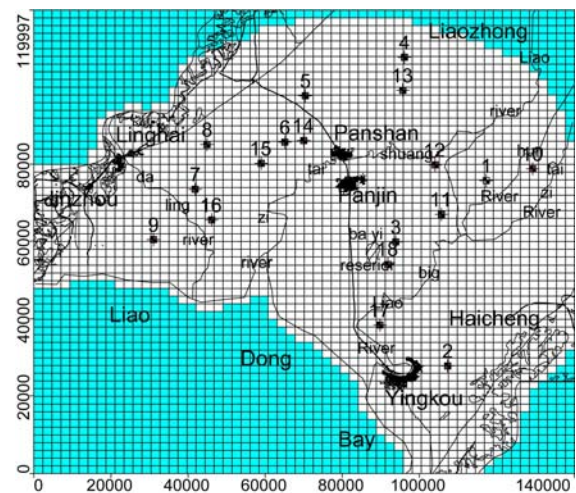

Fig. 8. Location of head observation wells (black dot points) used in model calibration.

other boundary the chloride concentration value was set at 0.05 kg/m^3. Throughout the computation, values of the chloride concentration in October, 2004 were assumed constant at the boundary conditions. The green color area is the inactive area

and the white color area represents the active area.

Table 3. Results of observed and calculated heads with residuals

Well ID	X-Model	Y-Model	Observed heads(m)	Calculated head(m)	Residuals (m)
1	117348.5	75583.8	2.8	3.449896	0.649896
2	107162	27707.3	4.1	2.848223	-1.25178
3	93919.5	59896.6	2.4	2.25253	-0.14747
4	96160.58	107569.5	3.5	4.329527	0.829527
5	70490.6	97586.7	3.7	2.791774	-0.90823
6	64989.9	85770.3	2.4	2.372885	-0.02712
7	41968.4	73342.8	2.6	3.311563	0.711563
8	44820.6	85159.2	3.7	3.208998	-0.491
9	31170.7	60304.1	2.5	3.822999	1.322999
10	129164.9	78843.53	-3.7	-2.79269	0.907314
11	105735.9	66823.46	-7.3	-8.87193	-1.57193
12	104106.1	79658.45	-6.5	-7.00136	-0.50136
13	95549.4	99216.5	-6.8	-5.52821	1.271788
14	70083.1	86177.8	-6.5	-7.1932	-0.6932
15	58877.9	80065.9	-9	-7.69063	1.309371
16	46246.7	65397.4	-8.3	-7.05188	1.24812
17	89844.9	38301.3	-6.6	-7.23111	-0.63111
18	91882.3	53988.5	-7.4	-8.88264	-1.48264

ranges from 3 to 80 m/day, while the resulting effective porosity from 0.14 to 0.3. It is noteworthy that the model calibration of this study is of preliminary nature due to the limited number and duration of the observation data. Additional model calibration shall be attempted when more field data become available in the future.

The simulated extent of seawater intrusion into the aquifer Layers A1, A2 and A4 in April, 2009 is depicted in Fig. 10. Compared with that in October, 2004, the extent of seawater intrusion was expanded, indicating that further seawater intrusion occurred from October, 2004 to April, 2009. As shown in Fig. 10, seawater intrusion in Layer A2 is considerably faster than that in Layers A1 and A3 in April, 2009.

correlation coefficient:0.982
mean error: 0.886
root mean square error: 0.987
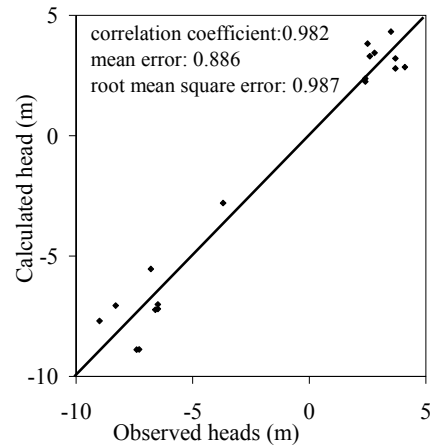
Fig. 9. Scatter diagram showing the relationship between the observed and calculated heads in April, 2009.

The simulated extent of seawater intrusion into the aquifer Layers A1, A2 and A4 in April, 2009 is depicted in Fig. 10. Compared with that in October, 2004, the extent of seawater intrusion was expanded, indicating that further seawater intrusion occurred from October, 2004 to April, 2009. As shown in Fig. 10, seawater intrusion in Layer A2 is considerably faster than that in Layers A1 and A3 in April, 2009.

IV. MODEL CALIBRATION

The model calibration was conducted through a trial-and-error approach by adjusting the zonation and values of the two key parameters, i.e., hydraulic conductivities and effective porosity. The hydraulic head value was computed using SEAWAT until it matches the observed value with a satisfactory level. However, due to the scarcity of observed chloride concentrations, no attempt was made to adjust several transport parameters including dispersivities and recharge rates. These values remained the same as the initial assigned value. Furthermore, because of the lack of continuously monitored hydraulic head data, the model was only calibrated against the observed hydraulic heads at the end of simulation. During calibration, a total of 18 observed hydraulic head values measured in April, 2009 were used. All the observation well locations are shown in Fig. 8. Model calibration was stopped when a reasonable match between the observed and calculated heads is achieved.

Figure 9 shows that an overall correlation coefficient of 0.982, a mean error of 0.886 m and a root mean square error of 0.987 m are obtained by the model calibration. This indicates a reasonably good match between the observed and calculated heads. Residuals between the observed and calculated heads are also listed in Table 3. After model calibration, the resulting horizontal hydraulic conductivity for Layers A1, A2 and A4

V. RESULTS OF SEAWATER INTRUSION AND DISCUSSIONS

Prediction of the extent of seawater intrusion in coastal aquifers in Liao Dong Bay coastal plain 40 years to come after April, 2009 was carried out by running the calibrated computation 40-year forwards with all the conditions assumed to remain the same as those in 2004. The predicted extents of seawater intrusion in Layers A1, A2 and A4 (Fig. 10) show the further seawater intrusion occurrence even if all the hydrogeological conditions remained constant. Figure 10(A) show that the maximum extent of seawater intrusion in Layer A1 will increase 4.3 km and Layer A2 will increase 6.2 km toward north in research area for 40 years. In the southwest and northeast area, the extent of seawater intrusion becomes smaller than in the other area. Compared with Fig. 10(A), 10(B) and 10(C), it can be described that the seawater intrusion in Layer

A2 becomes significantly faster than that in Layers A1 and A3. Figure 10(C) shows that the maximum extent of seawater intrusion in Minghuazhen group layer will increase 2.8 km toward northwest in research area, the highest velocity of seawater intrusion is 62.2 m/yr in Minghuazhen group aquifer of this study. The results of Li [26] show that in Minghuazhen group aquifer, the average seawater intrusion velocity is 3.066 m/yr, the velocity of high seawater intrusion area is between 18.7 and 364.3 m/yr. In Guantao group aquifer, the chloride concentration slightly defers from Li's results [26]. In this model, Guantao group aquifer is setting as bottom boundary.
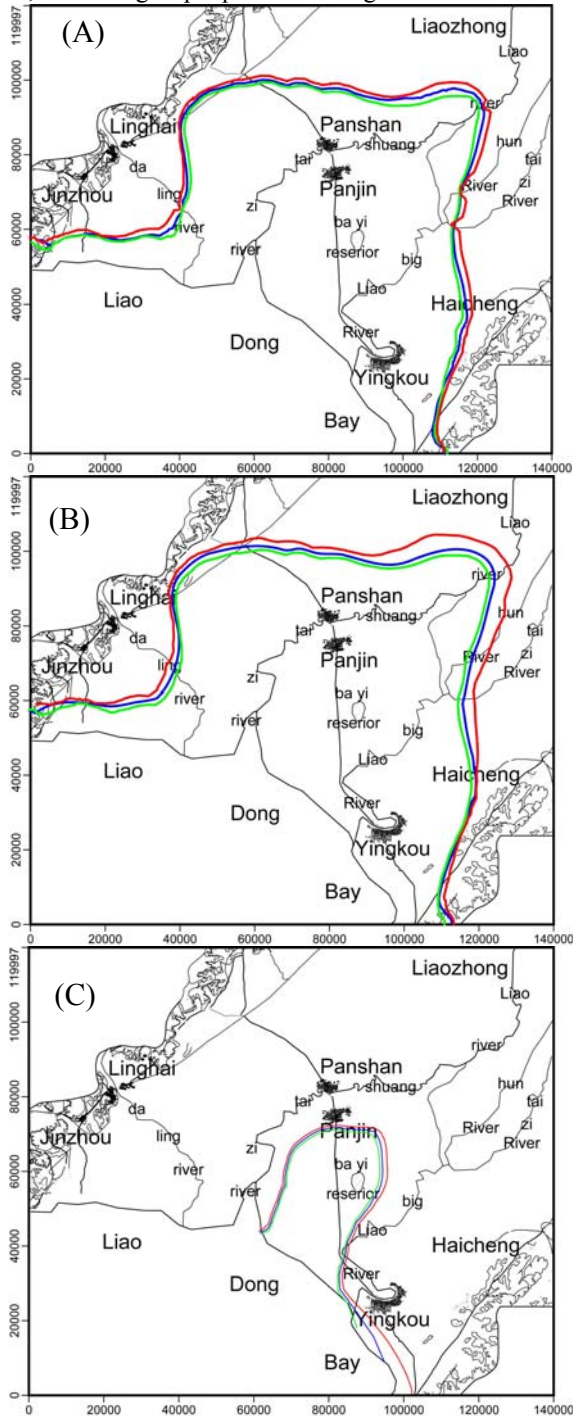
The predicted vertical distribution of chloride concentration in April, 2049 is shown in Fig. 11. For the left and right map, the green color area is the inactive area and the white area is the active area. For the left map, the red line on the left map shows the location of the cross-section. It shows that the intrusion occurred in two ways [28]: one is the advancement of the salt wedge at the bottom of the aquifer resulting from the density difference between salt water and fresh water (see Fig. 11, Layer A2). The other was the infiltration of salt water through the beach (see Fig. 11, Layer A1). It also can be described that the seawater intrusion in Layer A2 will become further than those in Layers A1 and A3.
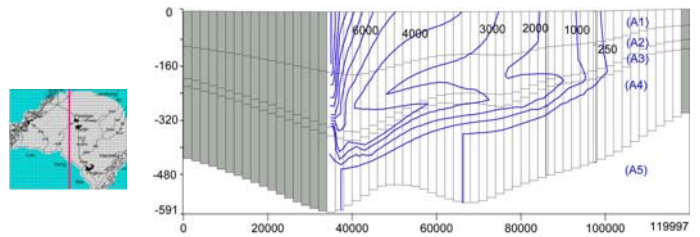

Fig. 11. The vertical distribution of chloride concentration in April, 2049 along the south-north cross-section with unit in g/m^3.

In the prediction model, all the conditions are assumed to remain same as those in October 2004. With the continuous population increase, the demand for groundwater pumping will increase. It can be expected the actual extent of seawater intrusion in future will be severer than the model prediction.

In this study, a quasi-three-dimensional model was constructed to simulate and predict the seawater intrusion in Liao Dong Bay coastal plain. To obtain a more realistic result, it is better to construct a three-dimensional model and using time series data to calibrate the model. For seawater intrusion, three-dimensional observation network for long-term observation is lacking in the study area. It is necessary to set up such observation network in this area. In addition, because of the lack of precise terrain data of the beach, this study considered ocean boundary as vertical beach slope. Ataie-Ashtiani et el [7] has done research to analyze the effect of the vertical beach slope and the sloping beach in seawater intrusion in unconfined aquifers. The results shows that in the steady-state case, the vertical beach slope results in a little further inland than the sloping beach case. In the further research, it is better to use a sloping beach ocean boundary.

This study did not consider the tidal effect on seawater intrusion and the effects of fluid viscosity variations caused by temperature changes [25]. The results of Ataie-Ashtiani et al. [7] showed that the tidal activity forces the seawater to intrude further inland and it also creates a thicker interface than the case without tidal effects in unconfined aquifers. Seven case studies have been done in his study to analyze the seawater intrusion effect by the saturated hydraulic conductivity, tidal

amplitude, regional hydraulic gradient and beach slope [7]. The effects of tidal, temperature variation and others sensitivity analysis of seawater intrusion should be emphasized in the further research.

Oude Essink construct a three-dimensional large-scale coastal aquifer in the northern part of the province Noord-Holland, the Netherlands to investigate its seawater intrusion. The entire groundwater system is covered by a grid with a surface of about 65.00 x 1.25 km^2. The sizes of horizontal element are 1250m x1250 m. [32]. Arlai et al. used the numerical model to investigate the seawater intrusion problem in the Bangkok Coastal Aquifer System with grid sizes varying from 2km x 2 km to 16km x 16 km [3, 4, 5, and 6]. In this model, it is a large-scale coastal aquifer, the plan model grid consists of the grid system of 60 columns and 60 rows with uniform spacing of 2.0 km (NS-direction) and 2.33 km (WE-direction), to save the hard disk and calculation time. Smaller grid size in the seawater intrusion simulation can deals with estimate the head values more accurate. Computation with smaller grid size and non-uniform grid (e.g. smaller grid size near the shore and larger at land side), may show some differences on the chloride concentration results. However, the trend of seawater intrusion might be almost the same. It is important to use the smaller grid size and non-uniform grid size to analyze small fluctuation of seawater intrusion in the simulation.

To protect the groundwater resources in the coastal aquifers of this study area from the seawater intrusion, regional water resources assessment and optimal allocation study should be done. It is recommended that some protection schemes, such as operational controls (e.g., pumping and well-construction restrictions) and engineering works (e.g., artificial recharge schemes and cut-off wall schemes), should be established based on the regional water resources assessment and optimal allocation study. Specifically, it is necessary to reduce the total amount of pumping groundwater in Minghuazhen group aquifer.

VI. SUMMARY AND CONCLUSIONS

Groundwater is the important source of freshwater in Liao Dong Bay coastal plain in Liao Ning, China, where 50% of the domestic water and the whole industrial water depend on the groundwater [11]. Therefore, it is imperative to protect groundwater from seawater intrusion in this area.

To predict the extent of seawater intrusion in future and provide useful information for the protection of groundwater resources, a quasi-three-dimensional numerical model of density-dependent groundwater flow and miscible salt transport was developed and assessed the future condition of seawater intrusion in the study area. The developed model incorporated regional geologic, geographic, and hydrogeological features. The model input parameters were determined from analysis of well logs, well driller's reports, and pumping tests. SEAWAT code was employed in the numerical study for the coupled density-dependent flow system, in which MODFLOW and MT3DMS were combined to simulate groundwater flow and

solute transport. The prediction results show that the maximum extent of seawater intrusion will increase 4.3 km in Layers A1 and will increase 6.2 km in Layers A2 toward north within 40 years. In the southwest and northeast area, the extent of seawater intrusion will increased smaller than other area. The seawater intrusion in Layer A2 was significantly faster than that in other two Layers. As a continuous increase in population, the demand for groundwater pumping might be more intensified. Then it can be expected the actual extent of seawater intrusion in future might be more severe than the model prediction. So it is very important to protect the freshwater aquifers from salt water contamination in the study area.

Due to the scarcity of the observed chloride concentrations and continuously monitored head data, the model can only calibrated by the hydraulic heads observed in April, 2009. For this calibration, a total of 18 observed hydraulic head values were used resulting in good agreement of the observed and calculated hydraulic heads. An additional calibration will be necessary in the future when more data became available.

This study constructed a new numerical model that can analyze and predict the extent of seawater intrusion in Liao Dong Bay coastal plain in both Quaternary and Neozoic layers. The main numerical code employed in the modeling is SEAWAT that is an effective tool for simulating variable-density flow and transport under complex geometries and geological settings. The developed computational model in this study may provide a valuable information for the study of seawater intrusion in coastal aquifers under similar hydrogeological conditions.

REFERENCES

1. Abd-Elhamid, H.F., and Javadi, A.A., "A density-dependant finite element model for analysis of saltwater intrusion in coastal aquifers," *Journal of Hydrology*, Vol. 401, pp. 259- 271 (2011).
2. Andersen, P. F., Mercer, J. W., and White, J. H. O., "Numerical modeling of salt-water intrusion at Hallandale, Florida," *Ground Water,* Vol. 26 (5), pp. 619–630 (1988).
3. Arlai, P., Koch, M., and Koontanakulvong, S. Modeling flow and transport for sustainable yield estimation of groundwater resources in the Bangkok aquifer system, *EGU General Assembly 2006, Vienna, Austria* (2006).
4. Arlai, P., Koch ,M. ,and Koontanakulvong, S. Statistical and Stochastic Approaches to Assess Reasonable Calibrated Parameters in a Complex Multi-Aquifer System, *Proceedings of CMWR XVI-Computational Methods in Water Resources, Copenhagen, Denmar,* (2006).
5. Arlai, P., Koch, M. ,and Koontanakulvong, S. Numerical Investigation of the Cradle of Saline Contamination and Effective Remediation Schemes for Amending Saline Water Pollution Problem in the Bangkok Coastal Aquifers System. *3rd APHW Conference, Bangkok,* (2006).
6. Arlai, P., Koch M., Koontanakulvong, S. ,and Weerapol, B. Numerical Modeling as a Tool to Investigate the Feasibility of Artificial Recharge to Prevent Possible Saltwater Intrusion into the Bangkok Coastal Aquifers System, *Proceedings of Groundwater Hydraulics in omplex Environments, Toulouse, France ,* (2006).

7. Ataie-Ashtiani, B., Volker, R.E., and Lockington, D.A., "Tidal effects on sea water intrusion in unconfined aquifers," *Journal of Hydrology,* Vol. 216, pp. 17–31 (1999).

8. Bakker, M., and Schaars, F., *The Sea Water Intrusion (SWI) Package Manual, Version 0.2*, University of Georgia, Athens (2003).

9. Bear, J., *Hydraulics of groundwater*, New York, McGraw-Hill, (1979).

10. Bhosale, D. and Kumar, C., Simulation of Seawater Intrusion in Ernakulam Coast, *proceeding of International Conference on Hydrology and Watershed Management, Hyderabad*, pp. 390-399, (2002).

11. Bian, J. M., and Tang, J. "Groundwater resources optimal allocation countermeasures in the liaohe oil field area," *Proceedings of the 34th Congress of International Association of Hydrogeologists*, Bejing,China, (2006).

12. Bobba, A.G., "Mathematical models for saltwater intrusion in coastal aquifers," *Water Resources Management*, Vol. 7: pp. 3–37 (1993).

13. El-Bihery, M. A., "Groundwater flow modeling of Quaternary aquifer Ras Sudr, Egypt," Environmental Geology, Vol. 58, pp. 1095–1105 (2009).

14. Evans, M., *Nutrient Discharge to Cockburn Sound from a Subterranean Mixing Zone: a Comparison of Transport and Reaction Timescales*, Honours thesis, University of Western Australia, (2005).

15. Giambastiani, B. M. S., Antonellini, M., Oude Essink, G. H. P., and Stuurman, R. J., "Saltwater intrusion in the unconfined coastal aquifer of Ravenna (Italy): A numerical model," *Journal of Hydrology,* Vol. 340, pp. 91-104 (2007).

16. Guo, W., and Bennett, G. D., "Simulation of saline/fresh water flows using MODFLOW," *Proceedings of MODFLOW '98 Conference At the TnternationalGround Water Modeling Center*, Colorado School of Mines, Golden, Colorado, vol 1, pp. 267–274 (1998a).

17. Guo, W. X., and Langevin, C. D., *User's Guide to SEAWAT: A Computer Program For the Simulation of Three-dimensional Variable-density Ground-water Flow*, USGS Techniques of Water Resources Investigations, Book 6, chap A7, (2002).

18. Harbaugh, A. W., Banta, E. R., Hill, M. C., and McDonald, M. G., *MODFLOW- 2000, the U.S. Geological Survey Modular Ground-Water Model—User Guide to Modularization Concepts and the Ground-Water Flow Processes*, U.S. Geological Survey Open- File Report 00-92, (2000).

19. Huyakorn, P. S., Andersen, P. F., Mercer, J. W., and White, J. H. O. "Saltwater intrusion in aquifers: Development and testing of a three-dimensional finite element model," *Water Resource Research,* Vol. 23, No. 2, pp. 293-312.

20. HydroGeoLogic Inc., *MODHMS—MODFLOW-Based Hydrologic Modeling System: Documentation and User's Guide*, Herndon, Virginia (2002).

21. Kopsiaftis, G., Mantoglou, A., and Giannoulopoulos, P., "Variable density coastal aquifer models with application to an aquifer on Thira Island," *Desalination*, Vol. 237, pp. 65–80 (2009).

22. Langevin, C. D., and Guo, W. X., "MODFLOW/MT3DMS-based simulation of variable-density ground water flow and transport," *Ground water*, Vol. 44, No. 3，pp. 339–351 (2006)

23. Langevin, C. D., Oude Essink, G. H. P., Panday, S., Bakker, M., Prommer, H., Swain, E. D., Jones, W., Beach, M., and Barcelo, M., "MODFLOW based tools for simulation of variable-density groundwater flow," In: Cheng A, Ouazar D (eds) *Coastal Aquifer Management: Monitoring, Modeling, and Case Studies*, Lewis Publishers, Boca Raton, pp. 49–76 (2004).

24. Langevin, C. D., Shoemaker, W. B., and Guo, W., *MODFLOW-2000, the U.S. Geological Survey Modular Ground-Water Model—Documentation of the SEAWAT-2000 Version With the Variabledensity Flow Process (VDF) And the Integrated MT3DMS Transport Process (IMT)*, USGS Open-File Report 03-426 (2003).

25. Langevin, C.D., Thorne, D.T., Jr., Dausman, A.M., Sukop, M.C., and Guo, W. X., *SEAWAT Version 4: A Computer Program for Simulation of Multi-Species Solute and Heat Transport*, U.S. Geological Survey Techniques and Methods Book 6, Chapter A22, (2007).

26. Li, Y. M., *Groundwater Quality Simulation and Forecast In Liaohe Oil Field*, (in chinese), Msc Thesis, Jiling University, 86 p (2005).

27. Lin, J., Snodsmith, J. B., Zheng, C. M., and Wu, J. F., "A modeling study of seawater intrusion in Alabama Gulf Coast, USA," *Environmental Geology*, 57: pp. 119–130 (2009).

28. Mao, X., Enot, P., Barry, D.A., Li, L., Binley, A., and Jeng, D. S., "Tidal influence on behaviour of a coastal aquifer adjacent to a low-relief estuary," *Journal of Hydrology*, 327, pp. 110-127 (2006).

29. McDonald, M. G., and Harbaugh, A. W., *A Modular Three-dimensional Finite-difference Ground-water Flow Model*, U.S. Geological Survey Techniques of Water Resources Investigations, Book 6, chap A1, (1988).

30. Ministry of Health of the Heople's Republic of China, Standards for drinking water quality, GB 5749-2006, p. 9 (2006).

31. Oude Essink, G. H. P., "MOC3D adapted to simulate 3D densitydependent groundwater flow," *Proceedings of MODFLOW '98 Conference At the International Ground Water Modeling Center*, Colorado School of Mines, Golden, Colorado, vol 1, pp. 291–300 (1998).

32. Oude Essink, G. H. P., "Saltwater Intrusion in 3D Large-Scale Aquifers: A Dutch Case," *Physics and Chemistry of the Earth, Part B: Hydrology, Oceans and Atmosphere*, Vol. 26, No. 4, pp. 337-344 (200l).

33. Sorek, S., and Pinder, G. F., "Survey of computer codes and case histories." In: Bear J et al (ed) *Seawater Intrusion In Coastal Aquifers: Concepts, Methods, and Practices*, Kluwer Academic Publishers, Dordrecht, pp. 399–461 (1999).

34. Voss, C., *SUTRA: A Finite-Element Simulation Model for Saturated-Unsaturated Fluid-Density-Dependent Ground-Water Flow With Energy Transport or Chemically-Reactive Single-Species Solute Transport*, Water Resources Investigation Report 84-4369, U.S. Geological Survey, (1984).

35. Wang, W. D., Zhang, G. X., and Li, B. L., *Report on Groundwater Management Simulation in Panjin City, Liaoning Province*, (in chinese), Liaoning Hydrogeology and Engineering Geology Exploration (1992).

36. Xue, X. D., The Research of the Simulation With Prediction of the Groundwater Level And the Rational Utilization of the Water Resource In Panjin Area, (in chinese), Msc Thesis, Jiling University, 91p (2005).

37. Zheng, C. M. and Wang, P. P., *MT3DMS: Documentation and User's Guide. Contract Report SERDP-99-1*, U.S. Army Engineer Research and Development Center, Vicksburg, MS, (1999).